Ultramicroscopy 231 (2021) 113287

Contents lists available at ScienceDirect

Ultramicroscopy

journal homepage: www.elsevier.com/locate/ultramic

A sorter for electrons based on magnetic elements

Giulio Pozzi [a,b], Paolo Rosi [c], Amir H. Tavabi [a,*], Ebrahim Karimi [d], Rafal E. Dunin-Borkowski [a], Vincenzo Grillo [c,e,**]

[a] Ernst Ruska-Centre for Microscopy and Spectroscopy with Electrons and Peter Grünberg Institute, Forschungszentrum Jülich, 52425 Jülich, Germany
[b] Department of Physics and Astronomy, University of Bologna, viale B. Pichat 6/2, 40127 Bologna, Italy
[c] Department FIM, University of Modena and Reggio Emilia, via G. Campi 213/a, 41125 Modena, Italy
[d] Department of Physics, University of Ottawa, 25 Templeton Street, Ottawa, Ontario K1N 6N5, Canada
[e] CNR-Institute of Nanoscience-S3, via G. Campi 213/a, 41125 Modena, Italy

ARTICLE INFO

Keywords:
Electron vortex beam
Magnetic phase plate
Electron optics
Electron orbital angular momentum
Sorter

ABSTRACT

The orbital angular momentum (OAM) sorter is an electron optical device for the measurement of an electron's OAM. It is based on two phase elements, which are referred to as an "unwrapper" and a "corrector" and are located in Fourier conjugate planes. The simplest implementation of the sorter is based on electrostatic phase elements, such as a charged needle for the unwrapper and electrodes with alternating charges or potentials for the corrector. Here, we use a formal analogy between phase shifts introduced by charges and vertical currents to propose alternative designs for the sorter elements, which are based on phase shifts introduced by magnetic fields. We use this concept to provide a general guide for phase element design, which promises to provide improved reliability of phase control in electron optics.

1. Introduction

A key strength of transmission electron microscopy is its ability to make use of information from both diffraction space and real space through the smart use of electron optics [1]. However, not long after the introduction of techniques such as electron magnetic circular dichroism [2], it became clear that electron microscopy requires a technique that can be used to measure an electron's orbital angular momentum (OAM) [3], which is neither a real space nor a diffraction space property. OAM is a quantum vectorial operator, whose component along the average propagation direction for a paraxial beam can be written in position representation as the azimuthal derivative of the wave. Its eigenstates are the now well-known vortex beams, whose phase winds in the azimuthal direction [4–7].

The introduction of electron vortex beams has triggered developments in physics that include new measurement tools [8–12]. Whereas the generation of OAM eigenstates is relatively simple, their measurement and decomposition has proved to be more cumbersome. In particular, methods that have been used to measure OAM composition [13–18] typically suffer from an inability to cleanly separate the radial and angular degrees of freedom of the electron beam [19].

A new device, which is referred to as an "OAM sorter", promises to overcome this problem by introducing a conformal transformation from Cartesian to polar coordinates to separate different OAM components [20–23]. The realization and application of this device is an active topic in electron optics. It has been realized using both holographic [21] and electrostatic [24] elements, based on theoretical concepts [22,23]. However, its implementation is still not straightforward as a result of practical problems. When using electrostatic elements, a needle-shaped electrode is typically used to perform the transformation, while a periodic array of alternatively-charged electrodes in the corresponding diffraction plane is used to correct the transformation phase. When using holograms, similar phase distributions can be imprinted directly in the form of thickness modulations of diffraction gratings. In the long term, a needle can become contaminated as a result of exposure to the electron beam, resulting in a change in its electrostatic field, whereas charging and wear can affect a grating material. In addition, the shape of a needle needs to be controlled accurately. Whereas a line of constant charge should be placed in the path of the electron beam, the device is in practice based on the use of conductive electrodes that can only be used to control potentials. A further problem in the electrostatic device results from a chromatic effect on the phase.

It is well known that magnetic lenses are less problematic than electrostatic lenses. Here, we introduce the concept of using magnetic fields as phase elements in the sorter by building on a formal analogy between the phase imparted to an electron beam by a charge

* Corresponding author.
** Corresponding author at: CNR-Institute of Nanoscience-S3, via G. Campi 213/a, 41125 Modena, Italy.
E-mail addresses: a.tavabi@fz-juelich.de (A.H. Tavabi), vincenzo.grillo@unimore.it (V. Grillo).

https://doi.org/10.1016/j.ultramic.2021.113287
Received 31 October 2020; Received in revised form 1 April 2021; Accepted 10 April 2021
Available online 21 April 2021

and a vertical current. This analogy, which has been suggested in recent experimental work [25,26], is presented systematically in the first section of this paper, in order to demonstrate that the effects of electrostatic phase elements can be reproduced by using either currents or permanent magnets. Key advantages of using a current are that it is more stable than a charge distribution, it can be controlled directly and its (magnetic) effect on the phase is independent of incident electron energy. After a short description of the operation of an ideal sorter device, we introduce new configurations of sorter elements that are based on currents and magnets. Just as for the electrostatic case, we discuss additional corrections that are required to remove residual astigmatism and we assess the experimental feasibility of the concept.

2. The ideal sorter

We begin by recalling, for the sake of completeness, the basic equations that describe an ideal sorter, first developed for light optics. The key component of the optical sorter transforms azimuthal position in the input beam into linear transverse position in the output beam, which is located in the Fraunhofer diffraction plane of the input beam. An input image comprising concentric circles is transformed into an output image of parallel lines. However, this transformation introduces a phase distortion that needs to be corrected by a second element. The complete system then comprises two optical elements, with the first element transforming the image and the second element correcting for phase distortions introduced by the first element. The second element is positioned in the Fourier plane of the first element, which can achieved by using a Fourier-transforming lens of focal length f [20].

The phase profile of the transforming optical element, which is referred to as an "unwrapper" or "sorter 1", is given by the expression

$$\phi_1(x,y) = \frac{d}{\lambda f}\left[y\arctan(x,y) - x\log\left(\frac{\sqrt{x^2+y^2}}{b}\right) + x\right], \tag{1}$$

which performs the conformal mapping $(x,y) \rightarrow (u,v)$ to its Fourier plane, with

$$u = -\frac{d}{2\pi}\log\left(\frac{\sqrt{x^2+y^2}}{b}\right) \tag{2}$$

and

$$v = \frac{d}{2\pi}\arctan(x,y). \tag{3}$$

In Eq. (1), λ is the wavelength of the incident electron beam, the parameter d is the length of the transformed beam, while b translates the transformed image in the u direction and can be chosen independently of d [20]. The function $\arctan(x,y)$ refers to the arc tangent of y/x, taking into account which quadrant the point (x,y) is in. The transforming optical element contains a half-line of discontinuity along the negative x axis, which defines the axis around which the OAM is measured and whose end corresponds to both the origin of the coordinate system and the location of the tip (see below).

The second optical element, which is referred to as the "corrector" or "sorter 2", introduces a phase correction of the form

$$\phi_2(u,v) = -\frac{db}{\lambda f}\exp\left(-2\pi\frac{u}{d}\right)\cos\left(2\pi\frac{v}{d}\right). \tag{4}$$

By adding a second Fourier transforming lens of focal length F after the phase correcting element, OAM states can be separated in its focal plane.

When using refractive elements instead of diffractive spatial light modulators, in order to have an efficient and compact mode transformer [27] it has been found to be convenient to add to ϕ_1 and ϕ_2 a thin convergent spherical lens of focal length f equal to the distance between the two elements, with the transmission function

$$\psi_f(x,y) = \exp\left[\frac{-i\pi(x^2+y^2)}{\lambda f}\right]. \tag{5}$$

3. Sorter elements based on currents

Whereas a phase shift can be introduced by a local variation in refractive index and relative optical distance in visible light optics, it is related to electromagnetic potentials in electron optics. According to the standard high energy phase object approximation [28], the electron optical phase shift $\varphi(x,y)$ can be written in the form

$$\varphi(x,y) = C_E\int_{-\infty}^{\infty} V(x,y,z)dz - \frac{2\,\pi\,e}{h}\int_{-\infty}^{\infty} A_z(x,y,z)dz\,, \tag{6}$$

where $C_E = \frac{2\pi}{\lambda}\frac{e}{E}\frac{E_0+E}{2E_0+E}$, e is the absolute value of the electron charge, h is Planck's constant, λ is the de Broglie electron wavelength, E is the electron's energy , E_0 is the electron's rest mass energy and $A_z(x,y,z)$ is the z component of the magnetic vector potential. The z axis of the coordinate system is aligned to the optical axis of the transmission electron microscope and has the same direction as the incident electron beam.

The equations that link V and A_z to their sources can be reduced to an identical form by noticing that (in the Coulomb Gauge)

$$\nabla^2 V = -\frac{\rho}{\epsilon_0} \tag{7}$$

and

$$\nabla^2 A_z = \mu_0 j_z\,, \tag{8}$$

where μ_0 is the vacuum permeability and the charge density ρ plays the same role as j_z, which describes the component of the current density parallel to the main propagation direction of the electron beam. According to these expressions, in-plane components of the current density do not contribute to the phase shift. They can eventually produce small, point-dependent wave translations, which can be neglected in most cases [25]. Taken together, the three equations show that, in the phase object approximation, the phase shift is proportional to the z integral of the potentials. The equation for the phase shift can then be written in the form [29]

$$\nabla_\perp^2\varphi = \frac{-C_E\,\sigma}{\epsilon_0} - \frac{2\pi\,e}{h}\,\mu_0\,\zeta\,, \tag{9}$$

where $\sigma = \int_{-\infty}^{+\infty}\rho dz$ and $\zeta = \int_{-\infty}^{+\infty} j_z dz$.

In this approximation, an inclined current in the plane x,z is equivalent to a vertical current j_z. A device that controls the phase using a charge distribution can therefore be reproduced by a series of vertical currents. This analogy is particularly relevant because it is often not the charge distribution but the equipotential distribution that can be controlled experimentally. Mathematically, the problem of finding appropriate boundary conditions for the potential in three dimensions can be transformed to the easier problem of finding projected sources of field in two dimensions. This difference is important when making conformal transformations of the electron wavefunction using harmonic phase elements, as suggested by Ruffato et al. [30].

Here, we use this analogy to propose new alternative OAM sorter phase elements, which are based on magnetostatic phase shifts. Their design is based simply on the substitution of charges by vertical currents, or by equivalent Ampere currents for magnetic materials. More broadly, the work of Ruffato et al. [30] provides a landscape of possible conformal transformations and a generalization of the sorter concept. The ultimate generalization would allow sorting of any set of wavefunctions, as recently proposed for visible light optics [31]. Unfortunately, the requirement for a harmonic phase does not allow the direct application of this formalism to electron optics and will require some modifications. Nevertheless, magnetic phase elements will be an essential ingredient in this direction.

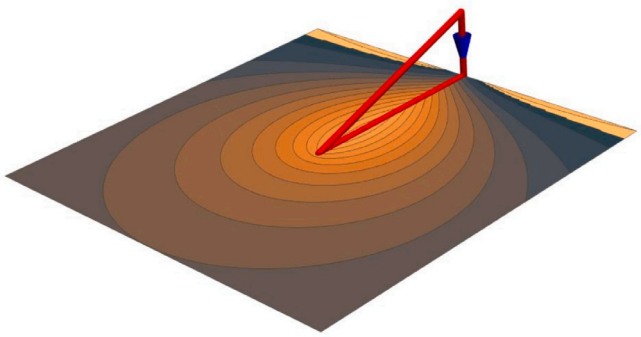

Fig. 1. Current circuit and corresponding phase shift for a magnetic sorter 1 element. The current closes just behind the element. See text for details.

3.1. Unwrapper or sorter 1

We begin by considering a closed circuit carrying current I between the tip of the device at O= $(0,0,0)$ and the points A= $(0,a,0)$ and B= $(0,a,c)$, as shown in Fig. 1.

In order to calculate the phase shift due to a straight section of the current-carrying wire at position $\mathbf{r}_P = (x_P, y_P, z_P)$ directed along $\mathrm{d}\mathbf{l} = (\mathrm{d}x_P, \mathrm{d}y_P, \mathrm{d}z_P)$ and, more generally, of a closed loop, we make use of the fifth formulation of Ampere's law in terms of the vector potential, according to the expression [32]:

$$\mathbf{A}_z(x,y,z) = -\frac{\mu_0}{4\pi} I \oint \frac{1}{r}\mathrm{d}\mathbf{l}\ , \tag{10}$$

where $r = \sqrt{(x-x_P)^2 + (y-y_P)^2 + (z-z_P)^2}$ and $\mathrm{d}\mathbf{l} = (dx_P, dy_P, dz_P)$.

As the phase shift described by Eq. (6) depends only on the z component of the vector potential, horizontal components of the wire can be neglected. It is convenient to parametrize the vertical segment OA in the form $\mathbf{r}_P = (0, a, c\ s)$, where $0 < s < 1$ and $\mathrm{d}\mathbf{l} = (0, 0, c\ \mathrm{d}s)$. Similarly, the oblique segment BO can be written $\mathbf{r}_P = (0, a\ s, c\ s)$, where $\mathrm{d}\mathbf{l} = (0, -a, -c)\mathrm{d}s$. The sum of the contributions of the two elements to the z component of the vector potential is therefore

$$\mathrm{d}\mathbf{A}_z(x,y,z) = \frac{\mu_0}{4\,\pi} I\ c\ \mathrm{d}s \left[\frac{1}{\sqrt{(x)^2 + (y-a)^2 + (z-c\ s)^2}} - \frac{1}{\sqrt{(x)^2 + (y-s\ a)^2 + (z-c\ s)^2}}\right]\ . \tag{11}$$

By making use of Eq. (6), we find for the contribution to the phase shift

$$\mathrm{d}\varphi(x,y) = \frac{e\ \mu_0}{2\ h} I\ c\ \mathrm{d}s \left\{\log(x^2 + (y-a)^2) - \log(x^2 + (y-a\ s)^2)\right\}\ . \tag{12}$$

The total phase shift is then obtained by integrating the above expression in $\mathrm{d}s$ between 0 and 1, resulting in the equation

$$\varphi(x,y) = \frac{c\ e\ \mu_0\ I}{2\ a\ h}\left(y\log\left((a-y)^2 + x^2\right) + 2x\arctan\left(\frac{y-a}{x}\right) + 2a - y\log\left(x^2+y^2\right) - 2x\arctan\left(\frac{y}{x}\right)\right)\ . \tag{13}$$

In the limit of large a, we can make the approximations

$$y\log\left((a-y)^2 + x^2\right) - y\log\left(x^2+y^2\right) \simeq -y\log\left(\frac{x^2+y^2}{a^2}\right) \tag{14}$$

and

$$2x\arctan\left(\frac{y-a}{x}\right) - 2x\arctan\left(\frac{y}{x}\right) \simeq -2x\ \mathrm{Sign}\ [a]\ \arctan[-\mathrm{Sign}[a]\ y, x]\ , \tag{15}$$

where $\mathrm{Sign}[x]$ is the sign function, so that

$$\varphi(x,y) = \frac{c\ e\ \mu_0\ I}{2\ a\ h}\left(-2x\ \mathrm{Sign}\ [a]\ \arctan[-\mathrm{Sign}[a]\ y, x] - y\log\left(\frac{x^2+y^2}{a^2}\right)\right)\ . \tag{16}$$

If constant and linear terms are neglected, then the functional phase shift of an ideal sorter described by Eq. (1) is recovered, once it is noted that the discontinuity is aligned along the y axis and lies on the positive or negative side depending on the sign of a. The result is identical to that obtained in the electrostatic case [23] if the charge distribution is substituted by the current according to the analogy described above, provided that

$$\frac{d}{\lambda f} = 2\ C_E\ C_V = \frac{c\ e\ \mu_0\ I}{a\ h}\ , \tag{17}$$

where $C_V = \frac{K}{4\pi\epsilon_0}$, K is the constant charge density of a charged line and ϵ_0 is the dielectric constant of vacuum.

3.2. Corrector or sorter 2

In this case, we consider two current distributions that have the shapes of a square wave and a sinusoid, as sketched in Fig. 2(a) and Fig. 3, respectively.

3.2.1. Square wave

A square wave current is equivalent to a periodic array of vertical wires at positions $(0, n\ d/2)$ carrying alternatively opposite currents, as the horizontal sections of the wire do not contribute to the phase. The phase shift of a single vertical wire of length $2L$ carrying current I at the origin [25] can be obtained from the first term of Eq. (12) with $a = 0$, in the form

$$\varphi(x,y) = \frac{e\ \mu_0}{h} I\, L \log\left[x^2 + y^2\right]\ . \tag{18}$$

Although it is a simple matter of addition to construct a finite square wave, it is more interesting to consider an infinite periodic arrangement of vertical wires at positions $(0, n\ d/2)$, which can be described by the expression

$$\sum (-1)^n \frac{e\ \mu_0}{h} I\ L \log\left[(x - n\frac{d}{2})^2 + y^2\right]\ . \tag{19}$$

As shown elsewhere, *e.g.*, in [33], this sum can be expressed analytically as

$$\varphi(x,y) = \frac{e\ \mu_0}{2h} I\ L \log\left(\frac{\cosh\left(\frac{2\pi y}{d}\right) - \cos\left(\frac{2\pi x}{d}\right)}{\cosh\left(\frac{2\pi y}{d}\right) + \cos\left(\frac{2\pi x}{d}\right)}\right)\ . \tag{20}$$

For $y \gg d$, the leading term in this Fourier series reads

$$\varphi(x,y) = \frac{2\ e\ \mu_0}{h} I\ L \exp\left(-\frac{2\pi|y|}{d}\right)\cos\left(\frac{2\pi x}{d}\right)\ . \tag{21}$$

Apart from a multiplying constant, this expression is coincident with the required functional form for sorter 2 described by Eq. (4). A cosine phase map of such an array is shown in Fig. 2(b).

3.2.2. Sinusoid

We describe a sinusoidal current by the parametric equation

$$\mathbf{r}_P = \left(x, 0, L\sin\left(\frac{2\pi x}{d}\right)\right)\ , \tag{22}$$

with

$$\mathrm{d}\mathbf{l} = \left(1, 0, L\frac{2\pi}{c}\cos\left(\frac{2\pi x}{d}\right)\right)\mathrm{d}x\ . \tag{23}$$

Even if the current is continuous, its z component varies as a cosine and it is equivalent to a cosine distribution of charges, resulting in the ability to generate the sorter phase explicitly without the need for approximations. The phase shift is then given by the expression

$$\varphi(x,y) = \frac{2e\mu_0}{h} I L \exp\left(-\frac{2\pi|y|}{d}\right)\cos\left(\frac{2\pi x}{d}\right)\ . \tag{24}$$

The current and corresponding phase shift are shown in Fig. 3.

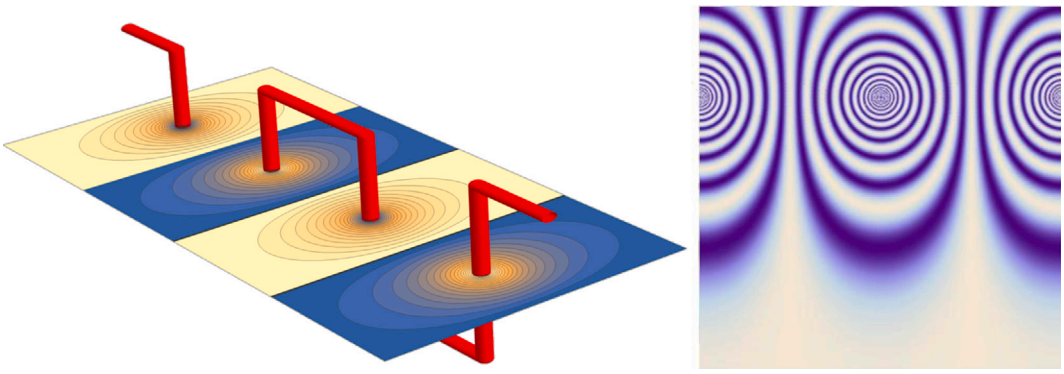

Fig. 2. Square wave current distribution suitable for the sorter 2 element. (a) Three-dimensional structure of the current, with a plane cutting it at half of the total amplitude and showing a contour map of the phase shift introduced by the current distribution. Blue and yellow correspond to opposite signs of the phase shift. (b) Cosine phase map calculated for a periodic distribution of vertical currents of opposite sign. See text for details. (For interpretation of the references to colour in this figure legend, the reader is referred to the web version of this article.)

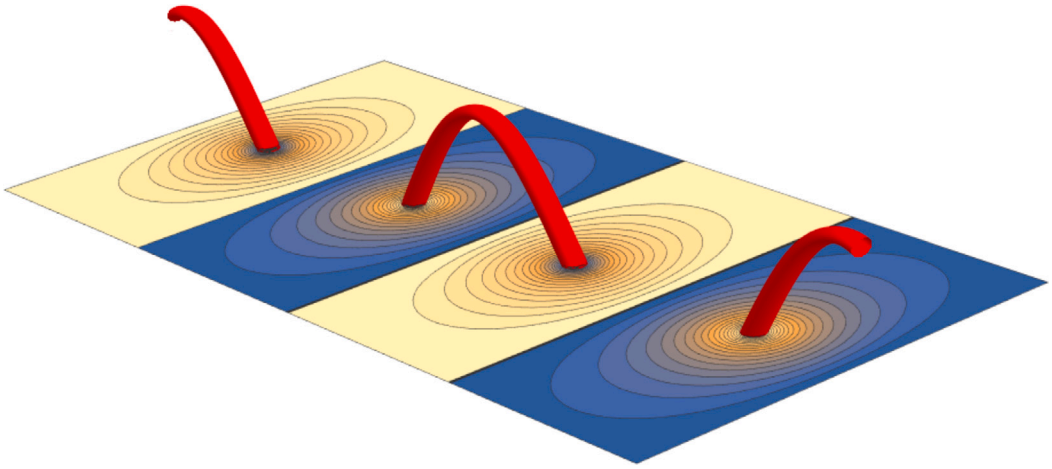

Fig. 3. Sinusoidal current distribution suitable for the sorter 2 element. The three-dimensional structure of the current is illustrated, with a plane cutting it at half of the total amplitude and showing a contour map of the phase shift introduced by the current distribution. Blue and yellow correspond to opposite signs of the phase shift. See text for details. (For interpretation of the references to colour in this figure legend, the reader is referred to the web version of this article.)

4. Sorter elements based on magnetic materials

4.1. Unwrapper or sorter 1

The magnetic effect of a current on the phase shift can be obtained equivalently from a magnetized element. The analogy is obtained by shaping the edge of the magnetized element based on the current distribution. We begin by considering a magnetic lamina of small thickness t with vertices at the points O= $(0,0,0)$, A= $(0,a,0)$ and B= $(0,a,c)$ and with a magnetization vector $\mathbf{M}$ in the x direction, *i.e.*, $\mathbf{M} = (M,0,0)$, as shown in Fig. 4. The magnetic vector potential of an elementary magnetic dipole with moment $\mathbf{m} = (m,0,0) = (M\ t\ dy\ dz,0,0)$, located at the origin of the coordinate system, is given by the expression [32]

$$A_z = \left\{0, -\frac{\mu_0\ m\ z}{4\pi\left(x^2+y^2+z^2\right)^{3/2}}, \frac{\mu_0\ m\ y}{4\pi\left(x^2+y^2+z^2\right)^{3/2}}\right\}\ , \tag{25}$$

where μ_0 is the vacuum permeability.

In the phase object approximation described by Eq. (6), the corresponding electron optical phase shift takes the form

$$\varphi(x,y) = -\frac{e\ \mu_0\ m\ y}{h\left(x^2+y^2\right)}\ . \tag{26}$$

As the phase shift does not depend on z, the contribution to the phase shift at the point (x,y) due to a column of dipoles at $(0,y_0,0)$ of height $y_0 = c/a$ (Fig. 4) is

$$d\varphi(x,y) = -\frac{c\ e\ \mu_0\ M\ t\ y_0(y-y_0)}{a\ h\left(x^2+(y-y_0)^2\right)}dy_0\ . \tag{27}$$

By integrating the above equation from 0 to a, the phase shift associated with the triangular magnetic lamina turns out to be

$$\varphi(x,y) = \frac{c\ e\ \mu_0\ M\ t}{2\ a\ h}\left(y\log\left((a-y)^2+x^2\right)+\right.$$
$$\left.2x\arctan\left(\frac{y-a}{x}\right)+2a-y\log\left(x^2+y^2\right)-2x\arctan\left(\frac{y}{x}\right)\right)\ . \tag{28}$$

By making use of the same approximations as in Eqs. (14) and (15), we obtain the expression

$$\varphi(x,y) = \frac{c\ e\ \mu_0\ M\ t}{2\ a\ h}\left(-2x\ \text{Sign}\ [a]\ \arctan[-\text{Sign}[a]\ y,x]\right.$$
$$\left.-y\log\left(\frac{x^2+y^2}{a^2}\right)\right)\ . \tag{29}$$

Therefore, by considering the correspondence between magnetization and Amperian currents, the magnetic device is shown to be equivalent to a current $I = -M\ t$ circulating on the edges of the lamella.

4.2. Corrector or sorter 2

As a result of the projection feature of the phase object approximation, any periodic structure is able to give, in vacuum, the phase

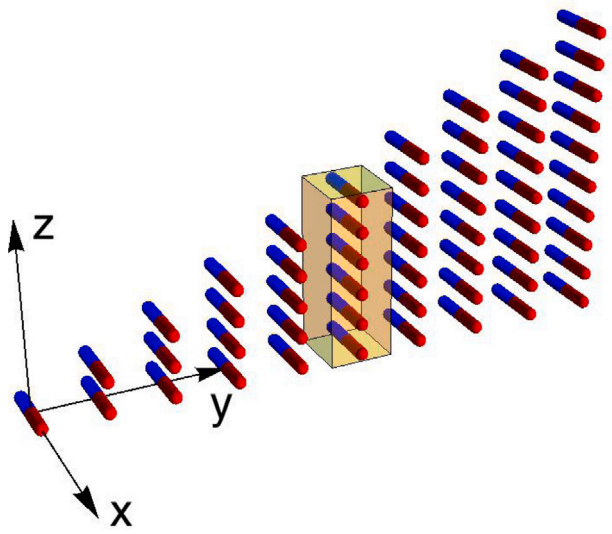

Fig. 4. Discrete representation of a continuous triangular distribution of elementary magnetic dipoles. The shaded prism represents a volume of integration along z.

shift required by the corrector element, or sorter 2, of the ideal sorter. We consider, as an illustrative example, a periodic array of alternating magnetic stripe domains of width w, aligned along y, in a thin specimen lying in the half-plane $x < 0$. The phase shift introduced by such an array (Fig. 5) has been calculated in analytical form previously [34] and is given by the expression

$$\varphi(x,y) = \frac{N}{2\pi}\,\Re\left(2e^{\frac{i\pi y}{w}}H(-x)\Phi\left(e^{\frac{2i\pi y}{w}},2,\frac{1}{2}\right) - \mathrm{Sign}(-x)e^{-\frac{\pi(|-x|-iy)}{w}}\Phi\left(e^{-\frac{2\pi(|-x|-iy)}{w}},2,\frac{1}{2}\right)\right), \tag{30}$$

where $N = \frac{2e\mu_0 M w t}{h}$ is the number of flux quanta trapped in the domain, t is the domain thickness, $H(x)$ is the Heaviside step function and $\Phi(z,s,a)$ is the Lerch transcendent function [35]. The phase shift of a basic period of this structure is shown in Fig. 5(a) for $N = 20$, illustrating the triangular shape of the phase in the specimen corresponding to the case of zero-width magnetic domain walls. The slow decrease in phase in the vacuum region is visualized more clearly in the form of a contour map in Fig. 5(b), from which the internal phase contribution has been removed.

The leading Fourier term in the former expression

$$\varphi(x,y) = \frac{4}{\pi}N\exp\left(-\pi\frac{x}{w}\right)\cos\left(\pi\frac{y}{w}\right) \tag{31}$$

has the analytical form required for sorter 2, as described in Eq. (4).

5. Design of a realistic sorter

In our former treatment of an electrostatic sorter [23], we recognized that the use of a line charge of finite length for sorter 1, combined with the need to have a mirror line for neutrality purposes, was responsible for an astigmatic contribution to the phase shift, which could wash out the sorting effect. We were able to compensate for this astigmatic contribution by adding two additional line charges (and their images) perpendicular to the line charge, thereby restoring the performance of the device. As magnetic elements do not, in general, require compensating mirror images, a simpler structure comprising only three elements (sorter 1 and two perpendicularly aligned elements) was investigated here. The results were disappointing, indicating that the mirror charges were also required for compensation.

In order to better appreciate the influence of astigmatism and its correction, we first consider a single magnetic element of length $a = 80$ μm (with the tip at the origin of the coordinate system) acting as sorter 1 in a device in which a length of the transformed beam of $d = 10$ μm over a focal length $f = 0.5$ m is required. These values are similar to the conditions used for our last experiments performed for an electrostatic sorter [24]. We are interested in a field of view of 30 μm × 30 μm centred on the tip.

As an illuminating beam, we consider a petal beam [21], which is defined by the equations

$$\psi_{ill} = \mathcal{N}\{\exp[i\ell\arctan(x,y)] + \exp[-i\ell\arctan(x,y)]\} \quad \text{for} \quad x^2+y^2 < R^2 \tag{32}$$

$$\psi_{ill} = 0 \quad \text{for} \quad x^2+y^2 > R^2, \tag{33}$$

where $\mathcal{N}$ is a normalization constant.

Fig. 6(a) shows the intensity distribution of the beam, with $R = 10$ μm and $\ell = 2$, in the sorter 1 plane, over a field of view of 30 μm × 30 μm. An amplitude function introduced to take into account the finite dimension of the device is also shown. The intensity before the sorter 2 plane is shown in Fig. 6(b). Four intensity minima are visible, corresponding to $\ell = \pm 2$. However, there is also a distortion caused by the finite dimensions of sorter 1. A Fraunhofer image calculated for

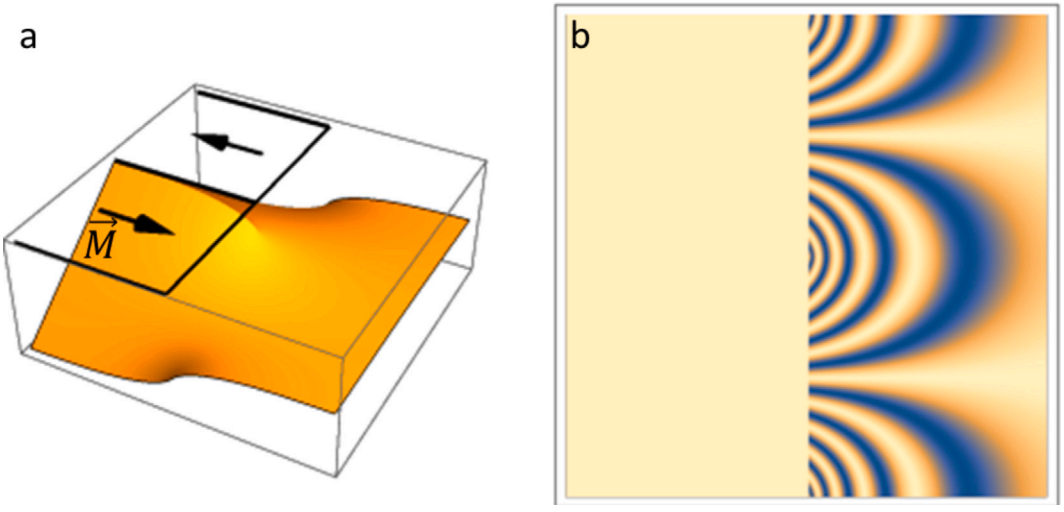

Fig. 5. (a) Three-dimensional representation of the phase shift for a basic period of an infinite array of alternately-oriented stripe domains aligned along the y direction in the half-plane $x < 0$.(b) Corresponding phase contour map in the vacuum region for $x > 0$.

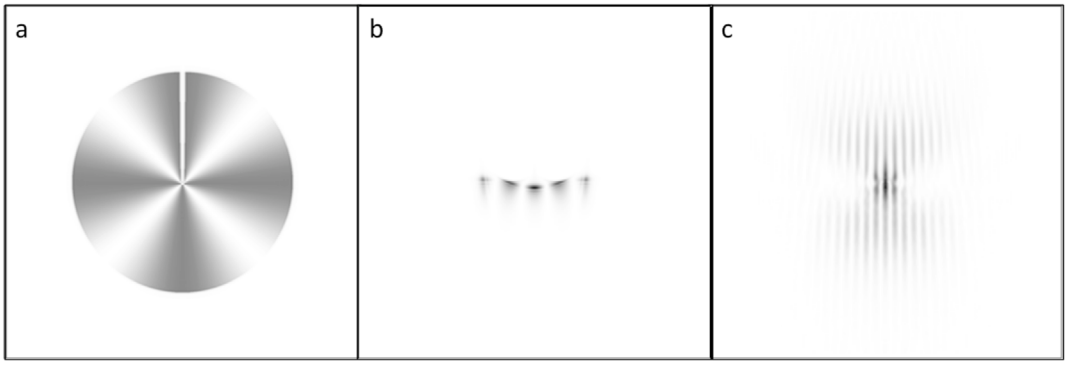

Fig. 6. (a) Petal beam with an OAM $|\ell| = 2$ intensity distribution. (b) Beam intensity distribution before the sorter 2 element and after it has interacted with the sorter 1 element. (c) Blurred OAM spectrum obtained without astigmatism compensation/correction.

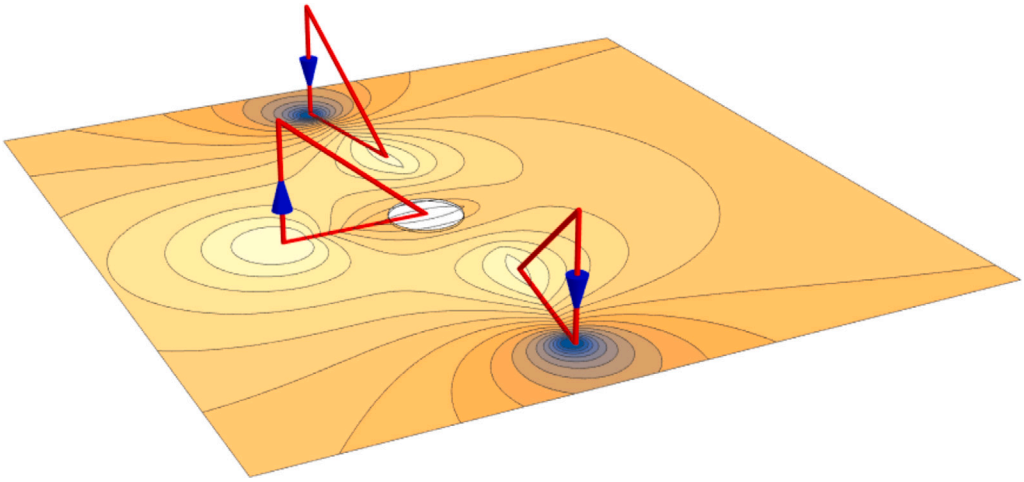

Fig. 7. Phase map calculated for sorter 1 with astigmatism correction elements. The currents of the sources are indicated schematically. The typical beam position is indicated by a circle.

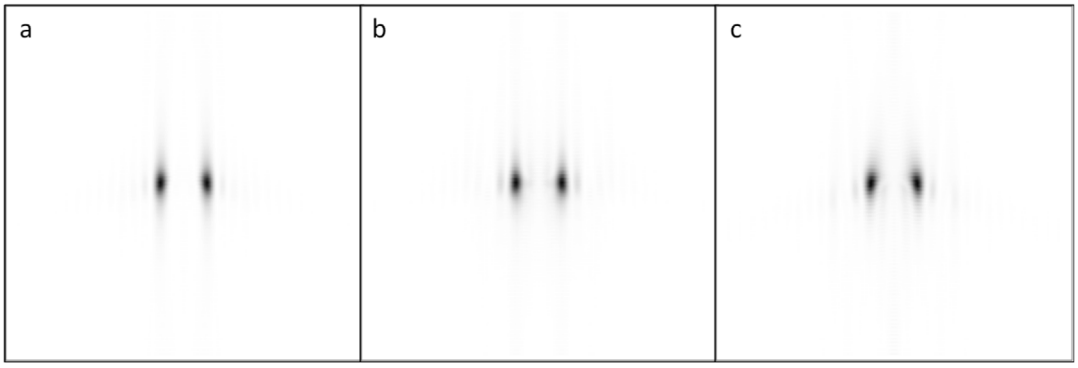

Fig. 8. OAM spectrum obtained using a magnetic sorter with a length of 80 μm and with a lateral astigmatism corrector oriented at an angle of: (a) 10° (corresponding to Fig. 7), (b) 0° and (c) 20°.

focal length $F = 2$ m in Fig. 6(c) shows that the astigmatism blurs the sorting effect completely.

In order to optimize the device without resorting to a replica of the electrostatic device, we introduced two additional magnetic elements at a distance of 40 μm, with their tips aligned with sorter 1. We then investigated the effect of rotating them with respect to sorter 1, as shown in Fig. 7. For two triangular elements with lengths of 80 μm, compensation is achieved at an angle of 10°, as shown in Fig. 8(a). The focal length of the Fraunhofer lens has been increased to $F = 5$ m, in order to emphasize the variations and features of the intensity distribution in the diffraction image. Deterioration of the image at 0 and 20° is shown in Fig. 8(b) and (c), respectively. We also tested the effect of placing the return vertical current at a greater distance and of having a trapezoidal instead of a triangular current circuit, but this modification was not as beneficial as the angular compensation.

We compared the results of Eq. (16) numerically with our previous experimental results for electrostatic sorter 1, where the average tilt of the beam was $\frac{d}{f} = 20$ μrad [24]. A similar result could be obtained for a current of 67 mA for the case $c = \frac{a}{2} = 40$ μm. Such a current requires detailed engineering, but is compatible with MEMS technology. For sorter 2 fabricated in the form of either a square wave or a sinusoidal current distribution, the minimum current required for correction, for

$z = 0$ in Eq. (21), is again 67 mA for $b = a = 80$ μm and $L = 20$ μm. It should be noted that for sorter 2 this is the minimum value required for correction. However, precise tuning is not required, since the position of the beam can be used to compensate for the exact phase, with the values of the parameters increased according to the exponential factor in Eq. (21). For the realization of sorter elements using magnetic materials, strong magnetic anisotropy is needed so that a slab of triangular or rectangular shape remains magnetized in the out-of-plane direction. For FePt, assuming a saturation magnetization of $M = 10^6$ A/m, a current of $I = 67$ mA corresponds to $t = 67$ nm for sorter 1. For the stripe domain configuration of sorter 2 (Eq. (31)) and the same value of magnetization M, minimum correction is achieved for a specimen thickness of 0.2 μm and a domain width $w = \frac{d}{2} = 5$ μm. These values correspond to the geometrical configuration considered above and should be changed for different geometrical parameters.

6. Conclusions

We have described an analogy between magnetic and electrostatic phase elements, which has general importance for fabricating customized phase elements, but is particularly relevant for the present case of an orbital angular momentum sorter. We have used analytical models to derive the shape of the current distribution that is required to achieve a completely magnetic version of the sorter. For the first sorting element, a new design with no direct analogue to the electrostatic case has been introduced to control the astigmatism that is introduced by the device. Numerical calculations indicate that phase shifts analogous to the electrostatic case can be obtained with currents that are within experimentally achievable ranges. The proposed devices have the important advantage that the field sources can be controlled directly, in contrast to the electrostatic case, for which the effective charge could only be controlled through the appropriate shaping of electrodes and by neglecting mutual induction of the elements. The new approach promises to provide a more accurate way to produce near-ideal OAM sorting over a large range of beam sizes.

Declaration of competing interest

One or more of the authors of this paper have disclosed potential or pertinent conflicts of interest, which may include receipt of payment, either direct or indirect, institutional support, or association with an entity in the biomedical field which may be perceived to have potential conflict of interest with this work. For full disclosure statements refer to https://doi.org/10.1016/j.ultramic.2021.113287. The Author declares that the author Prof. Dunin Borkowski is also Editor of this special issue

Acknowledgements

Q-SORT, the project leading to this paper, has received funding from the European Union's Horizon 2020 Research and Innovation Programme under grant agreement No 766970. This work has also received funding from the European Union's Horizon 2020 Research and Innovation programme (Grant No. 856538, project 3D MAGiC and Grant No. 823717, project ESTEEM3) and from the Deutsche Forschungsgemeinschaft (DFG, German Research Foundation) Project-ID 405553726 TRR 270.

References

[1] Helmut Kohl, Ludwig Reimer, Transmission Electron Microscopy: Physics of Image Formation, Springer, 2008.
[2] Peter Schattschneider, Stefano Rubino, Cécile Hébert, J. Rusz, J. Kuneš, P. Novák, E. Carlino, M. Fabrizioli, G. Panaccione, Giorgio Rossi, Detection of magnetic circular dichroism using a transmission electron microscope, Nature 441 (7092) (2006) 486–488.
[3] Johan Verbeeck, He Tian, Peter Schattschneider, Production and application of electron vortex beams, Nature 467 (7313) (2010) 301–304.
[4] Konstantin Yu Bliokh, Yury P. Bliokh, Sergey Savel'ev, Franco Nori, Semiclassical dynamics of electron wave packet states with phase vortices, Phys. Rev. Lett. 99 (19) (2007) 190404.
[5] Masaya Uchida, Akira Tonomura, Generation of electron beams carrying orbital angular momentum, Nature 464 (7289) (2010) 737–739.
[6] Benjamin J. McMorran, Amit Agrawal, Ian M. Anderson, Andrew A. Herzing, Henri J. Lezec, Jabez J. McClelland, John Unguris, Electron vortex beams with high quanta of orbital angular momentum, Science 331 (6014) (2011) 192–195.
[7] Vincenzo Grillo, Gian Carlo Gazzadi, Erfan Mafakheri, Stefano Frabboni, Ebrahim Karimi, Robert W. Boyd, Holographic generation of highly twisted electron beams, Phys. Rev. Lett. 114 (3) (2015) 034801.
[8] Jérémie Harris, Vincenzo Grillo, Erfan Mafakheri, Gian Carlo Gazzadi, Stefano Frabboni, Robert W. Boyd, Ebrahim Karimi, Structured quantum waves, Nat. Phys. 11 (8) (2015) 629–634.
[9] K.Y. Bliokh, I.P. Ivanov, G. Guzzinati, L. Clark, R. Van Boxem, A. Béché, R. Juchtmans, M.A. Alonso, P. Schattschneider, F. Nori, J. Verbeeck, Theory and applications of free-electron vortex states, Phys. Rep. 690 (2017) 1–70.
[10] S.M. Lloyd, M. Babiker, J. Yuan, Interaction of electron vortices and optical vortices with matter and processes of orbital angular momentum exchange, Rev. Modern Phys. 89 (2017) 035004.
[11] Benjamin J. McMorran, Amit Agrawal, Peter A. Ercius, Vincenzo Grillo, Andrew A. Herzing, Tyler R. Harvey, Martin Linck, Jordan S. Pierce, Origins and demonstrations of electrons with orbital angular momentum, Phil. Trans. R. Soc. A 375 (2087) (2017) 20150434.
[12] Vincenzo Grillo, Tyler R. Harvey, Federico Venturi, Jordan S. Pierce, Roberto Balboni, Frédéric Bouchard, Gian Carlo Gazzadi, Stefano Frabboni, Amir H. Tavabi, Zi-An Li, et al., Observation of nanoscale magnetic fields using twisted electron beams, Nature Commun. 8 (1) (2017) 1–6.
[13] Yoshiharu Saito, Shin-ichi Komatsu, Hitoshi Ohzu, Scale and rotation invariant real time optical correlator using computer generated hologram, Opt. Commun. 47 (1) (1983) 8–11.
[14] P. Schattschneider, M. Stöger-Pollach, J. Verbeeck, Novel vortex generator and mode converter for electron beams, Phys. Rev. Lett. 109 (8) (2012) 084801.
[15] Giulio Guzzinati, Laura Clark, Armand Béché, Jo Verbeeck, Measuring the orbital angular momentum of electron beams, Phys. Rev. A 89 (2) (2014) 025803.
[16] L. Clark, A. Béché, G. Guzzinati, J. Verbeeck, Quantitative measurement of orbital angular momentum in electron microscopy, Phys. Rev. A 89 (2014) 053818.
[17] Roy Shiloh, Yuval Tsur, Roei Remez, Yossi Lereah, Boris A. Malomed, Vladlen Shvedov, Cyril Hnatovsky, Wieslaw Krolikowski, Ady Arie, Unveiling the orbital angular momentum and acceleration of electron beams, Phys. Rev. Lett. 114 (9) (2015) 096102.
[18] Yuuki Noguchi, Shota Nakayama, Takafumi Ishida, Koh Saitoh, Masaya Uchida, Efficient measurement of the orbital-angular-momentum spectrum of an electron beam via a dammann vortex grating, Phys. Rev. A 12 (6) (2019) 064062.
[19] Hammam Qassim, Filippo M. Miatto, Juan P. Torres, Miles J. Padgett, Ebrahim Karimi, Robert W. Boyd, Limitations to the determination of a Laguerre–Gauss spectrum via projective, J. Opt. Soc. Amer. B 31 (6) (2014) A20–A23.
[20] Gregorius C.G. Berkhout, Martin P.J. Lavery, Johannes Courtial, Marco W. Beijersbergen, Miles J. Padgett, Efficient sorting of orbital angular momentum states of light, Phys. Rev. Lett. 105 (15) (2010) 153601.
[21] Vincenzo Grillo, Amir H. Tavabi, Federico Venturi, Hugo Larocque, Roberto Balboni, Gian Carlo Gazzadi, Stefano Frabboni, Peng-Han Lu, Erfan Mafakheri, Frédéric Bouchard, Rafal E. Dunin-Borkowski, Robert W. Boyd, Martin P.J. Lavery, Miles J. Padgett, Ebrahim Karimi, Measuring the orbital angular momentum spectrum of an electron beam, Nature Commun. 8 (2017).
[22] Benjamin J. McMorran, Tyler R. Harvey, Martin P.J. Lavery, Efficient sorting of free electron orbital angular momentum, New J. Phys. 19 (2) (2017) 023053.
[23] Giulio Pozzi, Vincenzo Grillo, Peng-Han Lu, Amir H. Tavabi, Ebrahim Karimi, Rafal E. Dunin-Borkowski, Design of electrostatic phase elements for sorting the orbital angular momentum of electrons, Ultramicroscopy 208 (2020) 112861.
[24] Amir H. Tavabi, Paolo Rosi, Giulio Pozzi, Alberto Roncaglia, Stefano Frabboni, Enzo Rotunno, Peng-Han Lu, Robert Nijland, Peter Tiemeijer, Ebrahim Karimi, Rafal E. Dunin-Borkowski, Vincenzo Grillo, Experimental demonstration of an electrostatic orbital angular momentum sorter for electrons, Phys. Rev. Lett. 126 (9) (2021) 094802.
[25] Amir H. Tavabi, Marco Beleggia, Vadim Migunov, Alexey Savenko, Ozan Öktem, Rafal E. Dunin-Borkowski, Giulio Pozzi, Tunable ampere phase plate for low dose imaging of biomolecular complexes, Sci. Rep. 8 (1) (2018) 1–5.
[26] Amir H. Tavabi, Hugo Larocque, Peng-Han Lu, Martial Duchamp, Vincenzo Grillo, Ebrahim Karimi, Rafal E. Dunin-Borkowski, Giulio Pozzi, Generation of electron vortices using nonexact electric fields, Phys. Rev. Research 2 (2020) 013185.
[27] Martin P.J. Lavery, David J. Robertson, Gregorius C.G. Berkhout, Gordon D. Love, Miles J. Padgett, Johannes Courtial, Refractive elements for the measurement of the orbital angular momentum of a single photon, Opt. Express 20 (3) (2012) 2110–2115.
[28] Giulio Pozzi, Particles and waves in electron optics and microscopy, in: Peter W. Hawkes (Ed.), Advances in Imaging and Electron Physics, Volume 194, Elsevier Academic Press, New York, NY, 2016.

[29] Vincenzo Grillo, Lorenzo Marrucci, Ebrahim Karimi, Riccardo Zanella, Enrico Santamato, Quantum simulation of a spin polarization device in an electron microscope, New J. Phys. 15 (9) (2013) 093026.
[30] Gianluca Ruffato, Enzo Rotunno, Vincenzo Grillo, A general framework for conformal transformations in electron optics, 2020, arXiv preprint arXiv:2003.09635.
[31] Nicolas K. Fontaine, Roland Ryf, Haoshuo Chen, David T. Neilson, Kwangwoong Kim, Joel Carpenter, Laguerre-Gaussian mode sorter, Nature Commun. 10 (1) (2019) 1865.
[32] William.T. Scott, The Physics of Electricity and Magnetism, second ed., Wiley, New York, 1966.
[33] E. Durand, Électrostatique, Volume 1, Masson, Paris, 1964.
[34] M. Beleggia, P.F. Fazzini, G. Pozzi, A fourier approach to fields and electron optical phase-shifts calculations, Ultramicroscopy 96 (1) (2003) 93–103.
[35] Stephen Wolfram, The Mathematica Book, fourth ed., Wolfram Media, Champaign, IL, 1999.